Acta Cryst. (1998). D**54**, 253–268

Crystallographic Study of Azurin from *Pseudomonas putida*

ZHI-WEI CHEN,[a] MICHAEL J. BARBER,[b] WILLIAM S. MCINTIRE[c,d] AND F. SCOTT MATHEWS[a]*

[a]*Department of Biochemistry and Molecular Biophysics, Washington University School of Medicine, St Louis, MO 63110, USA,* [b]*Department of Biochemistry and Molecular Biology, University of South Florida, College of Medicine, Tampa, Florida, USA,* [c]*Molecular Biology Division, Department of Veterans Affairs Medical Center, San Francisco, CA 94121, USA, and* [d]*Department of Biochemistry and Biophysics, and Department of Anesthesia, University of California, San Francisco, CA 94143, USA. E-mail: mathews@biochem.wustl.edu*

(*Received 3 May 1997; accepted 26 August 1997*)

Abstract

Azurin from *Pseudomonas putida* is a blue copper protein which functions as an electron carrier. Two crystal forms of azurin were grown, one in the presence and the other in the absence of zinc acetate; each belongs to space group $P2_1$ and contains two molecules per asymmetric unit. The zinc-free crystals have cell dimensions a = 43.25, b = 50.65, c = 54.60 Å, β = 107.79°, while the crystals grown from zinc-containing solution have cell dimensions a = 40.76, b = 51.22, c = 54.96 Å, β = 103.12°. The latter crystals were found to have four zinc ions incorporated into the crystal lattice. Both crystal structures were solved by the molecular-replacement method using the program *MERLOT*. The search model was the structure of azurin from *Alcaligenes denitrificans*. The crystallographic R factor for native azurin is 0.169 (R_{free} = 0.257) from 8 to 1.92 Å resolution, while that for zinc azurin is 0.181 (R_{free} = 0.248) from 10 to 1.6 Å resolution; for each structure the root-mean-square deviation in bond lengths from ideal values is 0.007 Å. In both crystal structures the Cu atom forms three strong bonds in the equatorial plane, two with $N^{\delta 1}$ from His46 and His117, and one with the thiolate S atom of Cys112. Two longer axial approaches are made by the S^{γ} from Met121 and the carbonyl O atom from Gly45. This results in a distorted trigonal bipyramidal coordination around the Cu atom. It further confirms the presence of a weak fifth bond to the copper in *P. putida* azurin, as with other azurin structures described at high resolution. The $N^{\delta 1}$ atom of His35 is protonated, as it is in the low-pH form of azurin from *Pseudomonas aeruginosa* but unlike the low-pH form of the azurins from *Alcaligenes denitrificans* or *Alcaligenes xylosoxidans*. In each crystal form the two molecules of azurin in the asymmetric unit are related by a local twofold axis and form a dimer stabilized by the interaction of a pair of hydrophobic patches surrounding the partially exposed His117 side chain. In the other known azurin crystal structures, analogous dimer formation is observed, but with different relative orientations of the molecules. The four zinc ions introduced during crystallization of zinc azurin are bound to the protein and participate in five- and sixfold ligand coordination with no affect on the copper binding site. The zinc ligands are N^{δ} from His, carboxylate O atoms from Asp and Glu, O^{γ} from Ser and water molecules. One of the zinc ions, located on a non-crystallographic twofold axis, links the dimers of the asymmetric unit into continuous chains parallel to the crystallographic (−101) direction and is primarily responsible for the altered unit-cell parameters. Two of the other zinc ions bind to His83, one in each molecule.

1. Introduction

The azurins are a subclass of the cupredoxin family of blue copper proteins which function as electron-transfer proteins in a variety of plants and bacteria. (For a review see Adman, 1991). Azurins are bacterial in origin and can function to transfer electrons from cytochrome c_{551} to nitrite reductase (van de Kamp *et al.*, 1990) or from aromatic amine dehydrogenase to cytochrome oxidase (Edwards *et al.*, 1995). The azurin from *Pseudomonas putida* (PP) is also capable *in vitro* of oxidizing substrate-reduced *p*-cresol methylhydroxylase (PCMH), a flavocytochrome *c*, and is believed to transfer electrons *in vivo* to the membrane-bound terminal cytochrome oxidase (Causer *et al.*, 1984).

High-resolution crystal structures of three bacterial azurins have been reported, from *Alcaligenes denitrificans* (AD) (Norris *et al.*, 1983; Baker, 1988), *P. aeruginosa* (PA) (Adman & Jensen, 1981; Nar *et al.*, 1991*a*), and *Alcaligenes xylosoxidans* (AX) (Korszun, 1987; Dodd *et al.*, 1995). The availability of site-directed mutants of these azurins has generated new interest in these model electron-transfer proteins and several reports on the properties of these mutants have been presented (van de Kamp *et al.*, 1990; Farver *et al.*, 1993; Murphy *et al.*, 1993; Romero *et al.*, 1993; Strange *et al.*, 1994; Hammann *et al.*, 1996). The crystal structures of apo-azurin (Nar, Messerschmidt *et al.*, 1992), metal-substituted azurins (Nar, Huber *et al.*, 1992; Blackwell *et al.*, 1994; Tsai, Sjölin, Langer, Bonander *et al.*, 1995) and several additional azurin mutants (Nar *et al.*, 1991*b*; Tsai, Sjölin, Langer, Pascher *et al.*, 1995) have further revealed

many structural details about the copper and its ligands. In addition, preliminary crystallographic studies of the azurin from *Pseudomonas fluorescens* have appeared (Zhu *et al.*, 1994), but structural details have not been reported.

The amino-acid sequence of azurin from *P. putida* has been determined by gas-phase sequencing methods (Barber *et al.*, 1993) and yields a calculated molecular mass of 13 783 Da. The sequence is 59% identical to azurin from AD, 67% identical to that from PA and 64% identical to that from AX (Fig. 1), the only other azurins whose high-resolution crystal structures are known. We report here the structure analysis of native and the zinc-containing crystals of azurin from PP at 1.92 and 1.6 Å, respectively, and a comparison of these structures with those of other azurins of known structure.

2. Materials and methods

2.1. *Crystallization and data collection*

Azurin was isolated from the bacterium *P. putida* and purified to homogeneity as described previously (Barber *et al.*, 1993). Crystals of azurin were grown by the hanging-drop method (Wlodawer *et al.*, 1975) at 277 K by mixing 5 µl protein at 10–15 mg ml^{-1} with 5µl 30–36% PEG 8000 solution containing 5 m*M* Tris–HCl buffer, pH 6.5–7.5 and 100 m*M* NaCl, both in the presence and in the absence of 180 m*M* zinc acetate. Both crystal forms belong to the monoclinic space group $P2_1$ and contain four azurin molecules per unit cell, giving a V_m of 2.0 Å^3 Da^{-1} (Matthews, 1968). The two crystal forms have distinctly different unit-cell parameters, shown in Table 1. Data were recorded on a Hamlin

Fig. 1. Comparison of amino-acid sequence for azurins. The sequences shown are for *Pseudomonas putida* (PP), *Alcaligenes denitrificans* (AD), *Pseudomonas aeruginosa* (PA) and *Alcaligenes xylosoxidans* (AX). This diagram was made using the program *Alscript* (Barton, 1993). Identical residues are contained within boxes and the residules forming ligands to copper are green.

Table 1. *Crystallographic data*

	Native azurin	Zinc azurin
Crystal size (mm)	1.0 × 0.27 × 0.15	0.8 × 0.5 × 0.3
pH	7.5	7.0
Space group	*P*21	*P*21
Unit-cell constants (Å, °)		
a	43.25	40.76
b	50.60	51.22
c	54.60	54.96
β	107.79	103.12°
Maximum resolution (Å)	1.92	1.6
No. of observations	56890	241088
No. of unique reflections	16127	27846
Data completeness (%)		
10–2.0 Å	99	—
2.06–1.92 Å	60	—
10–1.72 Å	—	99
1.72–1.60 Å	—	78
$\langle I/\sigma(I)\rangle$	11.7	10.7
$\langle I/\sigma(I)\rangle$ (max. res. shell)	2.5	1.9
$\langle Y/\sigma(Y)\rangle$†	19.4	23.1
$\langle Y/\sigma(Y)\rangle$† (max. res. shell)	3.0	2.8
R_{merge}‡ (%)	4.8	5.5
R_{merge} (%) (max. res. shell)	19.3	21.8

† $Y = \langle I_{hkl}\rangle$, the mean intensity for a given reflection. ‡ $R_{merge} = \sum_{hkl}\sum_i |I_i - \langle I\rangle| / \sum\langle I\rangle$, where I_i is the ith intensity measurement and $\langle I\rangle$ is the mean intensity for the reflection.

multiwire area detector (Hamlin, 1985) using graphite-monochromatized Cu $K\alpha$ radiation λ = 1.5418 Å) from a Rigaku RU-200 rotating-anode X-ray generator. The native and the zinc derivative (hereafter called zinc azurin) data sets were collected from one single crystal each at pH 7.5 and pH 7.0 and at resolution limits of 1.92 and 1.60 Å, respectively (Table 1).

2.2. *Protein coordinates*

The atomic coordinates for azurin from AD (entry No. 2AZA), AX (entry No. 1ARN) and PA (entry No. 4AZU) were obtained from the Protein Data Bank (Bernstein *et al.*, 1977).

2.3. *Structure solution*

Both structures were solved by molecular replacement using *MERLOT* (Fitzgerald, 1988) with the azurin from AD as the search molecule. Using data from 8 to 4 Å the cross-rotation functions gave unambiguous orientations for the two molecules in the asymmetric unit, with the correct solution corresponding to the two highest peaks, for both azurins. The translation searches also gave clear solutions for both structures. Ten cycles of rigid-body minimization gave R values of 0.446 and 0.475 for native and zinc azurin, respectively.

The native structure was refined initially using *PROLSQ* (Hendrickson & Konnert, 1980). Both structures were then refined by *X-PLOR*, *version* 3.1 (Brünger, 1992*a*), including several cycles of simulated annealing. Model building was carried out using the program package *TOM-FRODO* (Jones, 1985) on a Silicon Graphics workstation. In this step the AD sequence was replaced by the PP sequences of azurin. After rebuilding the model for three cycles, individual atomic B-factor refinement was introduced using the procedure given in the *X-PLOR version* 3.1 manual (Brünger, 1992*a*). Standard 'top 19' topology and electronic parameters for the polypeptide chain and locally derived (Cunane *et al.*, 1996) geometric and energy restraints on the copper coordination geometry (except for S^{γ} of Cys112 and O of Gly45) were employed in the early stages of refinement. Later in the refinement, non-crystallographic symmetry (NCS) restraints were introduced using NCS-weighting factors of 200 and 150 and NCS related B-factor restraints on ΔSigB of 1.0 and 1.5 for main-chain and side-chain atoms, respectively. The free R factor (Brünger, 1992*b*, 1993) was also introduced, using 10% of the reflections for the test data set. At that time topology and electronic parameters suggested by Engh & Huber (1991) were applied to the polypeptide, and the restraints on the Cu coordination geometry were removed. Four zinc ions were identified in difference Fourier maps of zinc azurin and were included in the model during the final stages of refinement. No restraints were applied to zinc or its ligands. Water molecules were introduced based on $F_o - F_c$ different map peaks >3.8σ; water molecules with B values greater than 65 Å^2 and in weak density in $2F_o - F_c$ map were removed. In the last cycle of refinement of both native and zinc azurin, NCS restraints were removed. Changes in the solvent-accessible surface area for azurin resulting from contact with other molecules in the crystal lattice were computed using *DSSP* (Kabsch & Sander, 1993). The criteria suggested by Baker & Hubbard (1984) were used to identify possible hydrogen bonds in both structures.

3. Results

3.1. *Structure analysis*

For zinc azurin, both molecules in the asymmetric unit were built independently, except for the first two residues at the N terminus. As one of the four zinc ions is bound to Glu2 of molecule *A*, the electron density at the N terminus of this molecule was much more clearly defined than that of molecule *B*, and these two residues could be placed with confidence. Subsequently, the coordinates for residues 1 and 2 for molecule *B* were obtained from molecule *A*. In native azurin, the electron density at the N termini of both molecules appeared weak and their coordinates were also generated from the zinc-azurin structure. Before NCS restraints were introduced into the refinement of both native and zinc azurins, alternate side-chain conformations were found on some surface residues, especially lysines. These alternate conformations generally disappeared after introduction of the NCS

Table 2. *Refinement result*

	Native azurin	Zinc azurin
Resolution range (Å)	8.0–1.92	10.0–1.6
No. of reflections	15874	27220
$R = (\|\|F_o\| - \|F_c\|\|)/\|F_o\|$ (%)	16.9	18.1
R(free)	25.7	24.8
Cutoff I/σ	<2.0	<1.5
No. of atoms		
Protein atoms (non-H)	1918	1918
Cu ions	2	2
Solvent molecules	163	222
Zn ions	—	4
Average temperature factor (Å^2)		
All atoms	25.86	17.99
Protein atoms	24.62	16.32
Solvent	40.42	32.24
Zn	—	24.85
R.m.s. $\|\Delta B\|$ for bonded atoms (Å^2)		
Main-chain atoms	1.36	1.03
Side-chain atoms	2.66	2.18
R.m.s. deviation from standard geometries		
Bond length (Å)	0.007	0.007
Bond angle (°)	1.020	0.975

restraints in the refinement and there are no alternate conformations included in either final structure.

There is no evidence to indicate that the Cu atoms in *P. putida* zinc azurin were replaced by zinc, either from any lessening of the deep blue color of the protein sample during crystallization or from the X-ray analysis. The $(F_o - F_c)$ map from zinc azurin, computed before any solvent molecules or zinc ions were introduced, showed 16 peaks above 5.4σ, none of which was located near the copper sites. In contrast, the crystal structure of zinc-substituted *P. aeruginosa* azurin, a by-product of heterologous expression in *Escherichia coli,* showed that the copper ion is replaced by zinc at the active site (Nar, Huber *et al.*, 1992). In that case the [F_o(zinc azurin) – F_o(native azurin)] difference electron density contained a positive peak with height 14.5σ located beside the Cu atom, indicative of a change in the metal-site geometry. The final model for native azurin consists of 1918 non-H protein atoms and 163 water molecules, giving R = 16.9% (R_{free} = 25.7%) from 8 to 1.92 Å resolution. The root-mean-square (r.m.s.) deviations from geometric ideality are 0.007 Å and 1.02° for bond lengths and angles, respectively. The model for the zinc azurin consists of 1918 non-H protein atoms, 222 water molecules and four zinc ions. The crystallographic residual, R = 18.1% (R_{free} = 24.8%) from 10 to 1.6 Å resolution with r.m.s. deviations from geometric ideality of 0.007 Å and 0.98° for bond lengths and angles, respectively. The two independent azurin molecules of each crystal form are very similar, with r.m.s. deviations of main-chain atoms of 0.24 Å for native and 0.20 Å for zinc azurin. The r.m.s. main-chain deviation between individual native and zinc azurins is 0.29 Å. The final refinement results are summarized in Table 2. There were no significant differences between the free R-factor with and without NCS restraints during refinement.

3.2. *Quality of the structure*

The Ramachandran plots of the φ/ψ values for individual residues of the native and zinc azurins are shown in Fig. 2. All residues lie within allowed regions, and 91.5 and 92.4%, respectively, of the non-glycine residues are located within the most favored regions. The remainder are in the additional allowed regions identified by Laskowski *et al.* (1993).

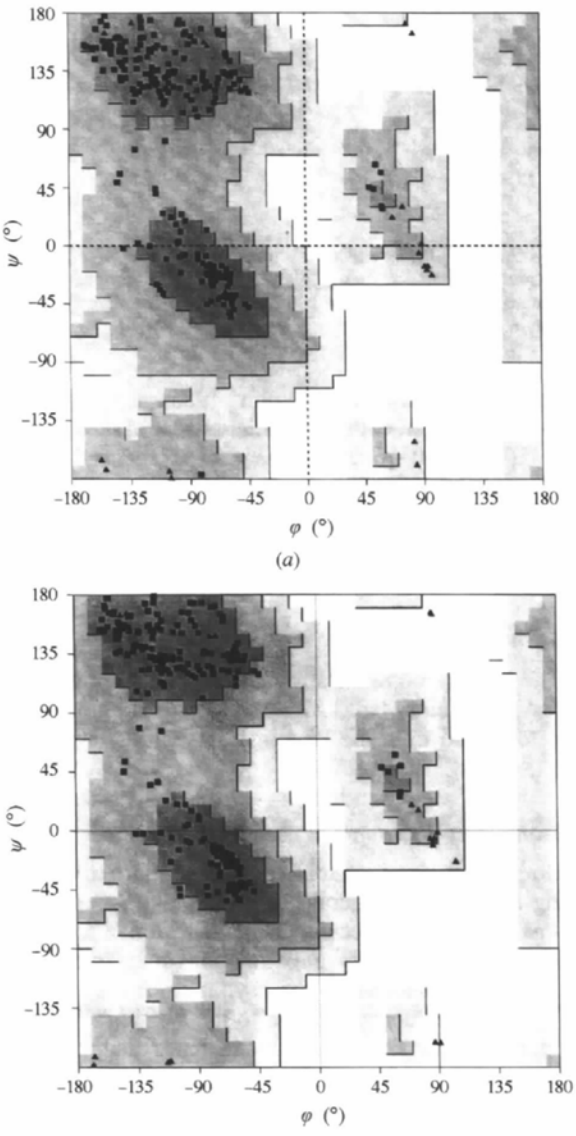

Fig. 2. Ramachandran plots for *P. putida* azurin. (*a*) Native azurin (both molecules); (*b*) zinc azurin (both molecules). Glycine residues are shown as filled triangles and all other residues as filled squares. The plots were calculated using *PROCHECK* (Laskowski *et al.*, 1993).

The average B values for main-chain atoms of each residue in molecules A and B are plotted in Fig. 3(a) for native azurin, and Fig. 3(b) for zinc azurin. The B-factor distribution for native azurin are similar in the two molecules of the asymmetric unit, with large values at both the N and C termini and in loops at residues 23–27 and 101–107. A similar situation exists in zinc azurin. However, the average B value for protein atoms in zinc azurin, 16 Å^2, is considerably lower than those in native azurin (25 Å^2; Table 2). Also, the B values for the 23–27 loop and the C terminus are markedly reduced in comparison with those of the N terminus and the 101–107 loop (see below). These results are consistent with the Wilson plots (Wilson, 1949) for both data sets which indicate overall B values of 20 and 14 Å^2 for native and zinc azurins, respectively. The refined crystal structures of azurins from AD, PA and AX show trends in B values similar to those in the PP azurin.

The electron density was generally well defined in each of the molecules, except for the first two residues and for some of the Lys and Asp side chains located on the surface, as well as a loop from residues 101 to 107 in the native azurin. The regions of poor electron density correlated with those having high B values. The electron-density map for zinc azurin at 1.6 Å resolution provided more structural detail than the map of native azurin (Fig. 4). The poorly defined residues and loops and the four zinc ions and their ligands were investigated by means of simulated-annealing omit maps. This helped to improve the fitting of the electron density for these residues and further confirmed the presence of the four zinc ions and their ligation pattern.

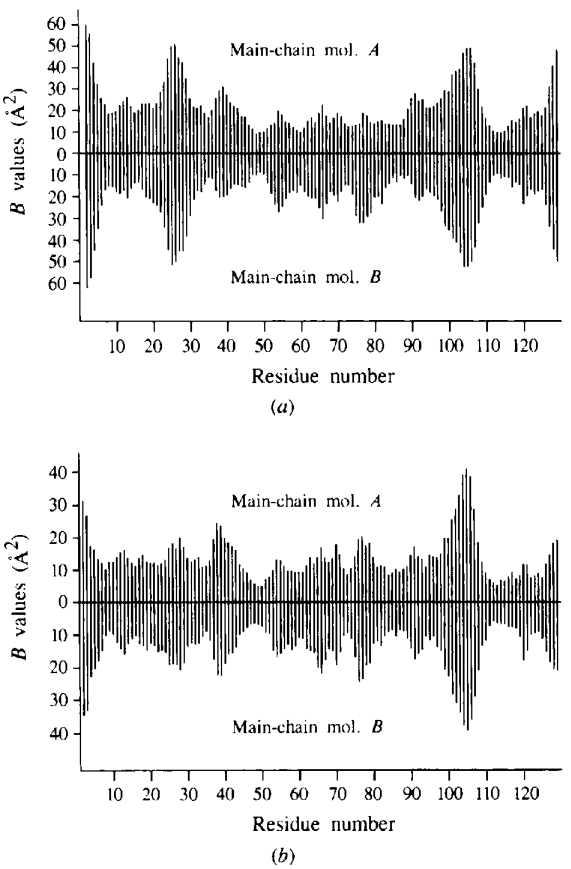

Fig. 3. Average temperature factors for main-chain atoms of molecule A (above the center line) and molecule B (below the center line) plotted *versus* amino-acid residue number. (a) Native azurin; (b) zinc azurin.

3.3. *Overall structure and comparison with other azurins*

A ribbon diagram of PP azurin is shown in Fig. 5. It consists of two β-sheets of four and five strands each which form a β clam shell. β-strand 2 forms the 'hinge' of the clam shell and is part of both sheets. The connection between β-strands 4 and 5 is interrupted by a helix/strand motif which forms an external flap. In addition, there is a single disulfide bridge connecting residues Cys3 and Cys26. This disulfide has been found in all azurins so far sequenced (Barber *et al.*, 1993). It can be reduced directly by CO_2 radicals produced during pulsed radiolysis experiments; this has suggested potential electron-transfer pathways from the disulfide bridge to copper site (Farver *et al.*, 1993).

Both forms of PP azurin are quite similar to the azurin from AD (Baker, 1988) used to solve the structure (Fig. 6). The r.m.s. deviation for main-chain atoms is 0.81 Å between native PP and AD azurins, and 0.78 Å between PP zinc azurin and AD azurin. The main differences occur at the N and C termini, residue 37 and in a loop from residues 103 to 109. The difference at position 37 arises from a reorientation of the plane of the peptide connecting residues 36 and 37 (see below). The PP azurin structure is also very similar to those of the other two refined azurin structures, from PA (Nar *et al.*, 1991*a*,*b*) and AX (Dodd *et al.*, 1995).

The copper site of azurin lies at the top of the β-barrel (as shown in Fig. 5) and is about 7 Å below the protein surface. The copper is five-coordinate, with three close ligands, His46 $N^{\delta 1}$, His117 $N^{\delta 1}$ and Cys112 S^{γ}, and two distant ligands, Met121 S^{γ} and Gly45 O; these five ligands form a distorted trigonal bipyramid (Table 3). Of the five copper ligands, only His117 is exposed to solvent to any extent, the remainder being buried. The exposed histidine is encompassed by a patch of nine hydrophobic residues, consisting of Met13, Leu39, Val43, Met44, Phe114, Pro115, Gly116, Ile118 and Met120. Each of the four His117 side chains in the two structures has a well defined water molecule bound at position $N^{\epsilon 2}$, at average hydrogen-bond distances of 2.67 Å and 2.80 Å and with average B values 19.4 and 14.5 Å^2 for native and zinc azurins, respectively. This area is a potential binding site for electron-transfer partners, as has been inferred from the structures of azurins from AD, PA and AX. An analogous site in the related cupredoxin ami-

cyanin has been observed to be the site for complex formation with its physiological electron donor methylamine dehydrogenase (Chen *et al.*, 1993, 1994).

The overall copper-site geometry is very similar to that found in other refined structures of azurins. Although the average C—N distance in native and zinc azurins is about 0.09 Å shorter than the average of those from the other three azurins, this deviation is probably within experimental error. The slight variation of C—S or C—O distances are also within experimental error.

3.4. *Intermolecular interactions*

In both native and zinc azurin the two molecules in each asymmetric unit are related by a non-crystallographic twofold axis perpendicular to the crystallographic *b* axis and to the (−101) diagonal of the respective monoclinic cell. This twofold symmetry is not exact. The r.m.s. deviation of equivalent Cα atoms is 1.76 and 1.65 Å for native and zinc azurins, respectively, when subunits *A* and *B* are superimposed onto subunits *B*

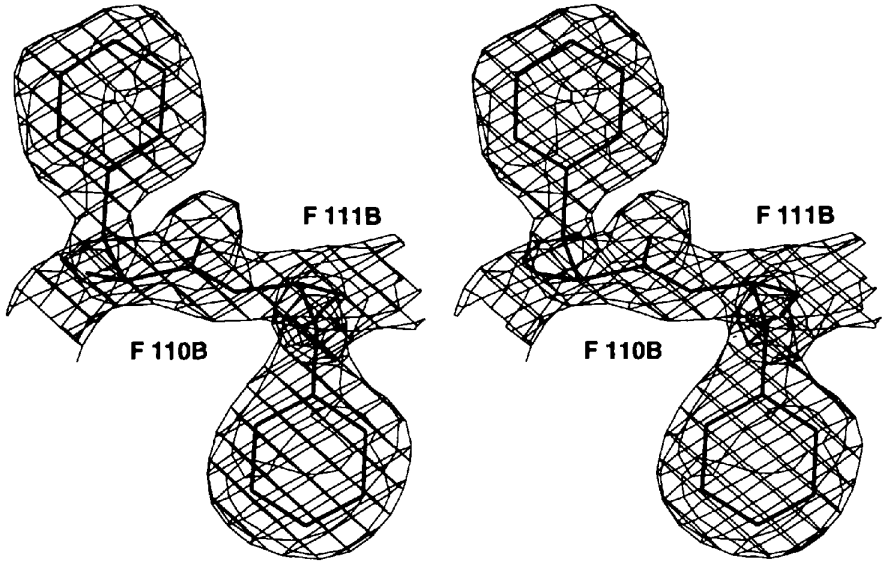

(*a*)

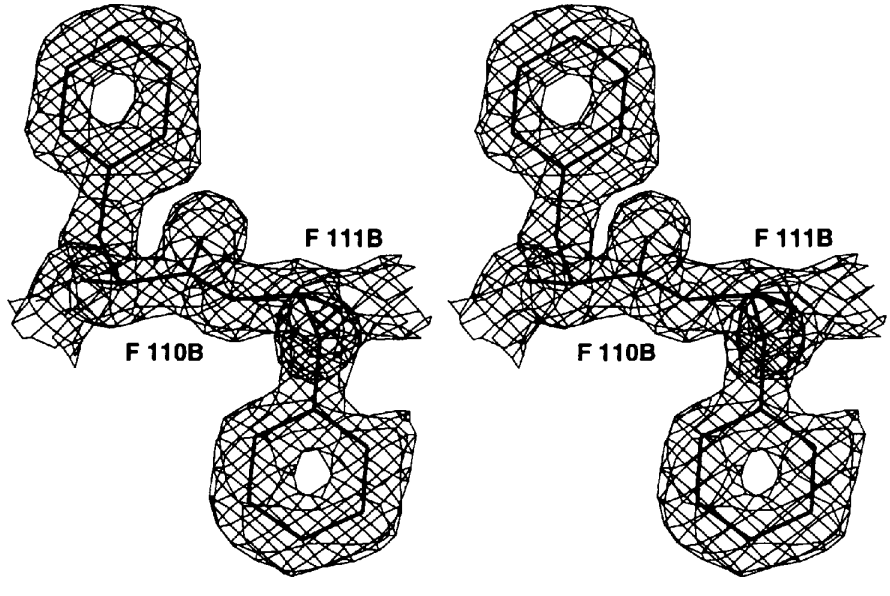

(*b*)

Fig. 4. Stereoview of the $2F_o - F_c$ electron-density map of two consecutive aromatic residues, Phe110*B* and Phe111*B*. (*a*) Native azurin at 1.92 Å resolution, contoured at 1.0σ; (*b*) zinc azurin at 1.60 Å resolution contoured at 1.0σ.

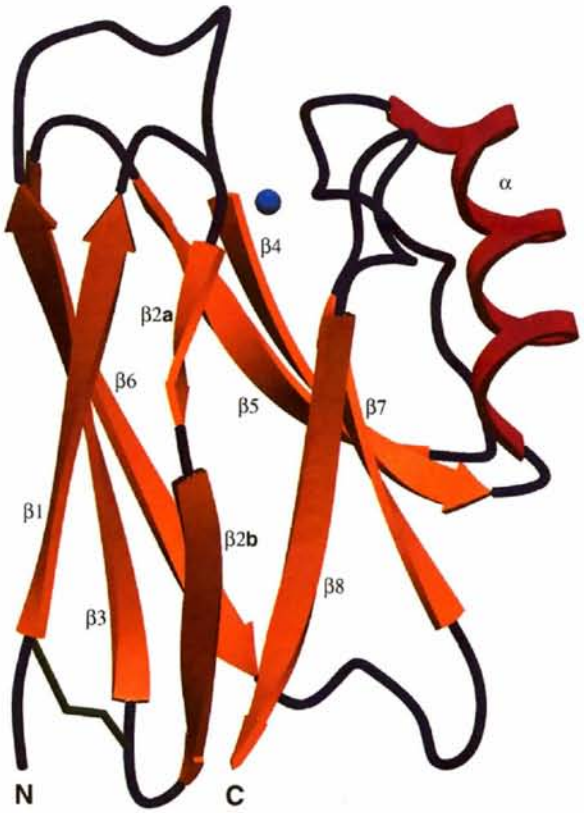

Fig. 5. Ribbon diagram of azurin from *P. putida*. β-strands are yellow, loops are red and the single helix is violet. The disulfide bridge linking strands β1 and the β2–β3 loop is shown in green.

and *A* of the same structure. However, the interactions between monomers are well conserved between the native and zinc structures. Both of these molecules are arranged with their hydrophobic patches, at the 'northern' end of the molecules, in mutual contact. In this configuration the two Cu atoms of each dimer are separated by 15.1 and 15.4 Å, respectively; the r.m.s. deviation between equivalent Cα atoms when the native and zinc dimers are superimposed is 0.40 Å.

The interface between the two azurin molecules occupies an area of approximately 500 $Å^2$ on each protein. There is only one hydrogen bond connecting the two molecules, in the zinc azurin only, between Asn42*A* $N^{\delta 2}$ and Met120*B* S^{δ}. There is no corresponding hydrogen bond between Asn42*B* and Met20*A* in zinc azurin because of the inexactness of the NCS. There are five water molecules buried within the interface (Fig. 7*a*). These five waters are conserved in the native and zinc-azurin structures, as are most of the van der Waals interactions between the monomers. Near the center of the interface are the two waters, described above, which are hydrogen bonded to the exposed $N^{\varepsilon 2}$ of the copper ligands His117*A* and His117*B*, respectively. They are also hydrogen bonded to the carbonyl O atoms of Val43*A* and Val43*B*. These two waters are then linked to a third water which is then linked sequentially to two more waters, 4 and 5, leading to the edge of the interface (Fig. 7*b*). The outermost water, No. 5, bridges the two azurin molecules, forming a hydrogen bond to Asn42*A* O and Gly116*B* O, respectively. In zinc azurin, this water is hydrogen bonded to an additional water beyond the dimer interface; in the native azurin the latter water is absent.

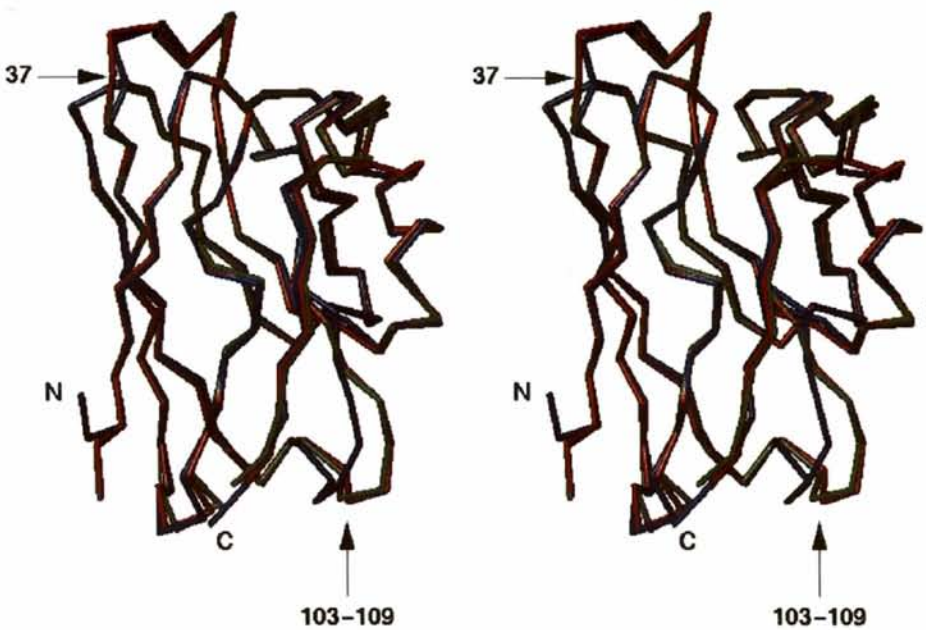

Fig. 6. Superposition of Cα diagrams of azurin monomers from *A. denitrificans* (blue) and of native azurin (red) and zinc azurin (green) from *P. putida*. The r.m.s. deviation for main-chain atoms is 0.81 Å for native *P. putida versus A. denitrificans* azurins and 0.78 Å for zinc azurin from *P. putida versus A. denitrificans* azurin. Residue 37 and the loops from residues 103 to 109, where the differences are greatest, are indicated.

Table 3. *Copper-site geometry in azurins*

	Native azurin (PP)		Zinc azurin (PP)		AzAD†	AzAX†	AzPA†
	Mol. 1	Mol. 2	Mol. 1	Mol. 2			
(*a*) Cu—ligand bond lengths (Å)							
Cu—$N^{\delta1}$(46)	2.01	1.93	1.96	1.91	2.08	2.02	2.03
Cu—$N^{\delta1}$(117)	1.94	1.96	1.94	1.94	2.01	2.02	2.11
Cu—S^{γ}(112)	2.13	2.13	2.13	2.12	2.12	2.12	2.25
Cu—S^{δ}(121)	3.01	3.14	2.95	3.07	3.12	3.26	3.15
Cu—O(45)	3.16	2.95	3.20	3.08	3.16	2.75	2.97
(*b*) Ligand—Cu—ligand bond angles (°)							
$N^{\delta1}$(46)—Cu—S^{γ}(112)	131.87	131.43	135.89	135.69			
$N^{\delta1}$(46)—Cu—$N^{\delta1}$(117)	106.59	102.51	103.20	103.54			
$N^{\delta1}$(46)—Cu—S^{δ}(121)	79.84	77.55	78.97	75.50			
S^{γ}(112)—Cu—$N^{\delta1}$(117)	118.52	124.77	116.75	119.61			
S^{γ}(112)—Cu—S^{δ}(121)	111.80	109.38	112.89	110.57			
$S^{\delta1}$(117)—Cu—S^{δ}(121)	93.25	90.63	95.75	91.74			
O(45)—Cu—S^{δ}(121)	142.85	144.62	145.24	146.39			
O(45)—Cu—$N^{\delta1}$(46)	66.16	69.68	69.48	74.03			
O(45)—Cu—S^{γ}(112)	102.19	102.25	100.06	101.10			
O(45)—Cu—$N^{\delta1}$(117)	83.00	83.93	78.16	81.93			

† AzAD, azurin from AD; AzAX, azurin from AX; AzPA, azurin from PA. All data for Cu–ligand bond lengths of AzAD, AzAX and AzPA are from Dodd *et al.* (1995).

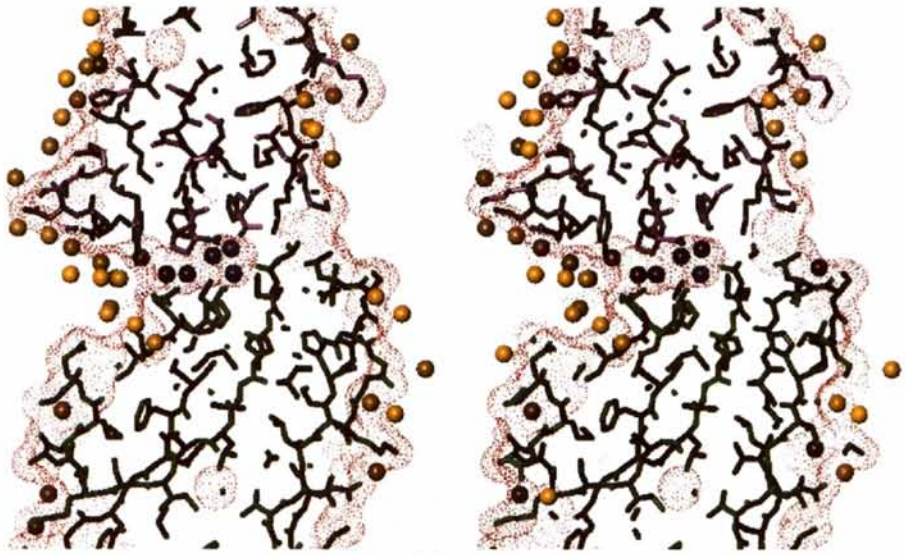

(*a*)

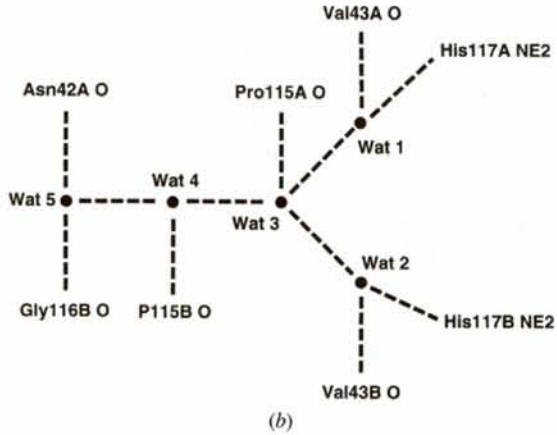

(*b*)

Fig. 7. (*a*) Slab section through the two monomers of zinc azurin from *P. putida* in the asymmetric unit showing the solvent-accessible surface (Connolly, 1983) as a dotted red surface. Five water molecules buried in the interface between molecules are shown as large blue spheres. Molecule *A* (upper) is violet and molecule *B* (lower) is green. Additional water molecules are shown as large yellow spheres. (*b*) Hydrogen-bonding interactions of the five buried water molecules in the interface between monomers of *P. putida* azurin.

Waters 3 and 4, are each bound to a single carbonyl O atom on opposite azurin molecules, at residues P115*A* and P115*B*, respectively.

A 'head-to-head' interaction of the two dimers is common to all four azurin structures determined so far. In each case, two azurin molecules are associated by either crystallographic or non-crystallographic twofold symmetry mainly through contact of their respective hydrophobic patches. However, there are three distinct modes of association between monomers among the various dimer structures (Fig. 8). If the azurin monomers are considered as ellipsoids, then the different modes of dimer association are defined both by differing angles between major axes and by differing relative rotations about these axes. The two dimers of PP azurin (both the native and zinc-bound forms) associate in one orientation, those of PA azurin (both molecules in the asymmetric unit) associate in a second orientation and the dimers of AX and AD azurin associate in a third manner, almost identically with each other. This association involves interactions among four loops which include the hydrophobic patch and are composed of residues 11–13 (loop 1), 39–43 (loop 2), 63–72 (loop 3) and 115–120 (loop 4). The interaction between the loop at the dimer interface of PP, PA and AD azurins are summarized in matrix form in Fig. 9. In all three azurins, there is extensive interaction between loops 2 and 4 of the NCS-related molecules. In PP azurin, additional NCS contacts involve interaction of loop 1 with 2, loop 3 with 4, and of loops 3 and 4 with themselves. In AD azurin, extensive interaction of loop 4 with itself occurs plus additional interactions of loops 1 and 3 with loop 4, and with themselves. In PA azurin, the additional interactions are localized to loops 1 with 4, 2 with 3, and of loops 1 and 2 with themselves. The angular relationships of molecule *B* to *A* in each of the azurin structures can be summarized by the polar angles relating molecules *B* in these azurins when molecules *A* are superimposed (Fig. 8). The three *B* molecules can be superimposed on each other by simple rotations, about axes which are nearly collinear, of approximately 150° to rotate PA onto PP, 45° to rotate AD onto PP and about 105° to rotate PA onto AD.

The contact surface areas of all dimers are on average about 500 ± 20 Å^2 per monomer. The greatest contact area occurs for AD azurin (523 Å^2) and the smallest for PP zinc azurin (478 Å^2). In all cases except AX (which has only a monomer in the asymmetric unit), there are slight differences in the contact surface areas, both overall and for individual residues, between individual monomers in a dimer, which results from slight deviations from exact twofold symmetry for these dimers. All the dimers contain ~16 amino-acid residues per monomer within the dimer interface (as defined by having reduced solvent accessibility in the dimer), almost all of which are common to all four azurins.

There is a 'tail-to-tail' interaction between the two monomers in adjacent unit cells of the zinc-azurin structure. This interaction is mediated by the major zinc

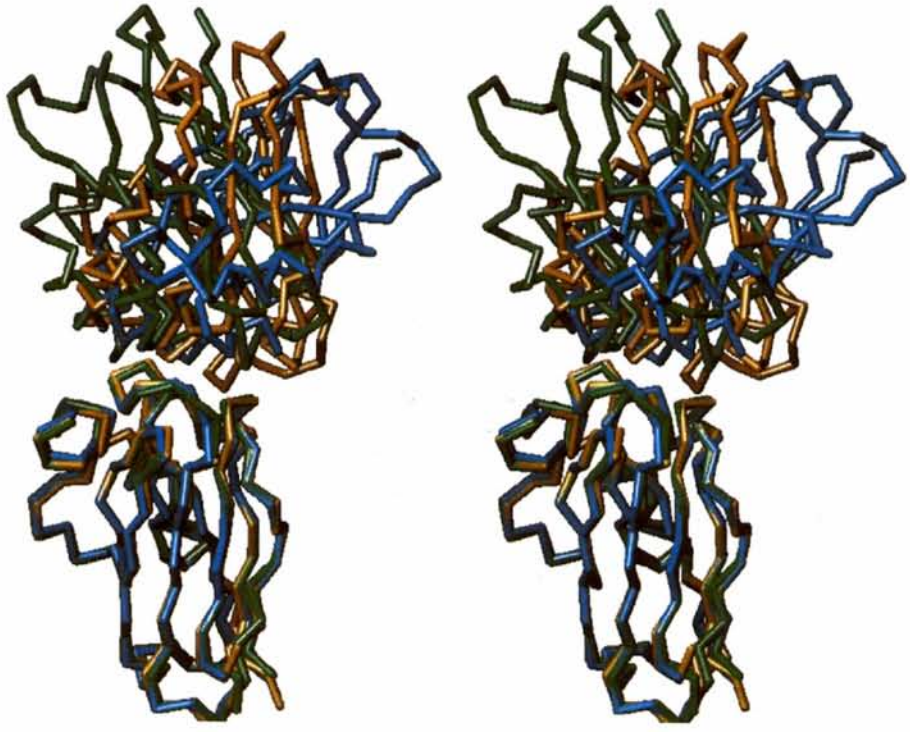

Fig. 8. Cα tracing of three pairs of azurin dimers from PP (green), AD (yellow) and PA (blue). Monomer *A* of the three azurin structures has been optimally superimposed. The three distinct orientations of molecule *B* of the three 'dimers' are apparent and reflect differences in their intermolecular interactions. Molecule *B* of PA and of AD azurin can be superimposed onto that of PP azurin by application of the coordinate transformation represented by the polar coordinates $\kappa = 150.6$, $\varphi = 45.5$, $\psi = 117.1°$ and $\kappa = 46.2$, $\varphi = 51.8$, $\psi = 128.2°$, respectively. Molecule *B* of PA can be superimposed onto molecule *B* of AD using the polar coordinates $\kappa = 105.5$, $\varphi = 50.6$, $\psi = 113.2°$. The relationship of two monomers of AX azurin (not shown) is very similar to that of AD azurin.

ion binding site, which is located on the alternate NCS axes of the unit cell. It includes two side-chain-to-side-chain hydrogen bonds between molecules, from Ser25*A* O^{γ} to Lys128*B* $O^{\tau 1}$#† and the NCS-related contact, as well as two bridging water molecules (Fig. 10). The two waters bridge the side-chain atoms of Asp23*A* $O^{\delta 2}$ and Lys128*B* $O^{\tau 2}$# and the NCS-related pair. The two water molecules, and the two O atoms of Ser25*A* O^{γ} and Asp23*A* $O^{\delta 1}$ from each molecule, form an octahedral coordination of the major zinc site (see below). These interactions help stabilize these portions of the zinc-azurin structure, as reflected in the diminished temperature factors of the 23–27 loop and the C-terminus of zinc azurin relative to the native azurin (Fig. 3).

3.5. *Hydrogen bonding*

The β clam shell of azurin consists of two β-sheets containing mixed antiparallel and parallel strands. Its hydrogen-bonding pattern is shown in Fig. 11. 25 hydrogen bonds are found in antiparallel β-bridges and 13 hydrogen bonds are found in parallel β-bridges. These hydrogen bonds are very similar to those found in the three other refined azurin structures. There are 27 side-chain-to-main-chain intramolecular hydrogen bonds in both native and zinc azurins. Most of these correspond to equivalent interactions in azurins from AD, PA and AX. A few differences in hydrogen bonding arise. Compared with azurin from AD, two are absent from PP, namely Tyr15 $O^{\eta}\cdots$Asn47 O and Tyr110 $O^{\eta}\cdots$Leu17 O. Compared with azurin from PA, two others are absent from PP azurin, namely Ser66 $O^{\gamma}\cdots$Asp62 O and Ser89 - $O^{\gamma}\cdots$Gly37 O. In the azurin from AX, there is a hydrogen bond between Asp62 $O^{\delta 1}$ and Ala58 O which is absent from PP, PA and AD azurin. All of these differences, except for the last one, arise from sequence differences among these three azurins; PP azurin has Phe in position 15 and 110, and Ala in positions 66 and 89, resulting in the loss of the respective hydrogen-bonding partner. However, the loss of these hydrogen bonds does not lead to any pronounced change in the structure around these residues. It was also found that that the hydrogen bond between His35 $N^{\delta 1}$ and Ser36 O, where the electron density is clear in both PP structures (Fig. 12), is not present in azurins from AD and AX, where instead a hydrogen bond is formed: His35 $N^{\delta 1}\cdots$Gly37 N. However, in PA, both types of hydrogen bond are observed, the former at pH 5.5 and the latter at pH 9.0 (Nar *et al.*, 1991*a*). This alteration in hydrogen-bonding arrangements corresponds to alternate orientations of the peptide bond between residues 35 and 36 and reflects differences in the protonation state of the His35 $N^{\delta 1}$ atom. There are 14 side-chain-to-side-chain

† The # symbol represents azurin residues related by crystallographic symmetry to those in the asymmetric unit.

PP Azurin

1	2	3	4	Loop #
0	5	0	0	1
	0	0	15	2
		2	3	3
			2	4

PA Azurin

1	2	3	4	Loop #
2	0	0	3	1
	4	4	10	2
		0	0	3
			0	4

AD Azurin

1	2	3	4	Loop #
2	0	0	3	1
	0	0	10	2
		2	2	3
			11	4

Fig. 9. Matrices indicating the number of contacts less than 4 Å between atoms of each of the four loops at the 'head-to-head' dimer interface between NCS-related molecules of PP, PA and AD azurins. Loops 1–4 consist of residues 11–13, 39–43, 63–72 and 115–120, respectively. Loops 1, 2 and 4 are located between β-strands 1–2, 3–4, and 6–7, respectively (Fig. 5) and contain the hydrophobic patch surrounding the copper site. Loop 3 is located at the C-terminal end of the single α-helix of azurin.

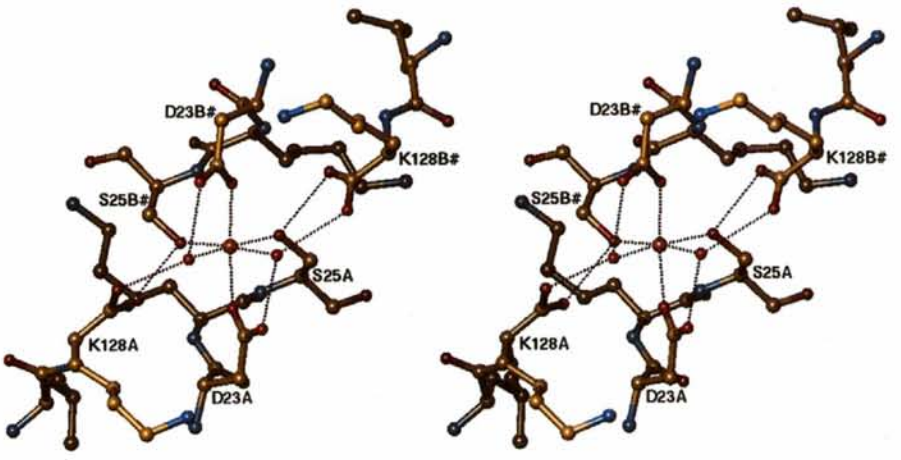

Fig. 10. 'Tail-to-tail' interaction of the two monomers of zinc azurin related by the non-crystallographic twofold symmetry. The zinc ion (yellow–brown) is octahedrally coordinated by carboxylate O atoms from Asp23*A* and Asp23*B*# (where # indicates a symmetry-related molecule), Ser25*A* and Ser25*B*# and by two water molecules (shown as isolated red spheres). In addition, the C-terminal carboxylates of Lys128*A* and Lys128*B*# are linked to Ser25*B*# and Ser25*A*, respectively. Each of the two water molecules also bridges the remaining carboxylate atoms of Asp25*A*, Lys128*B*# (C-terminus), and of Asp25*B*, Lys128*A*#, respectively.

intramolecular hydrogen bonds in both native and zinc azurins. Of these, three are salt bridges. The side chain of Arg79 is sandwiched between Asp62 and Asp77, forming three strong hydrogen bonds. These three residues are invariant and form salt bridges in all refined azurin structures, indicating their important stabilizing influence on this region. Another salt bridge links Lys4 and Glu32. It is interesting to note that in AD azurin Glu4 and His32 form a salt bridge; it would also seem to be possible to form a salt bridge between Glu4 and His32 in AX azurin if the side chain of the latter rotated by 180° (based on modeling using the atomic coordinates) with respect to azurin from PP. Apart from the salt bridge involving Arg79 common to all the refined azurins, there are four

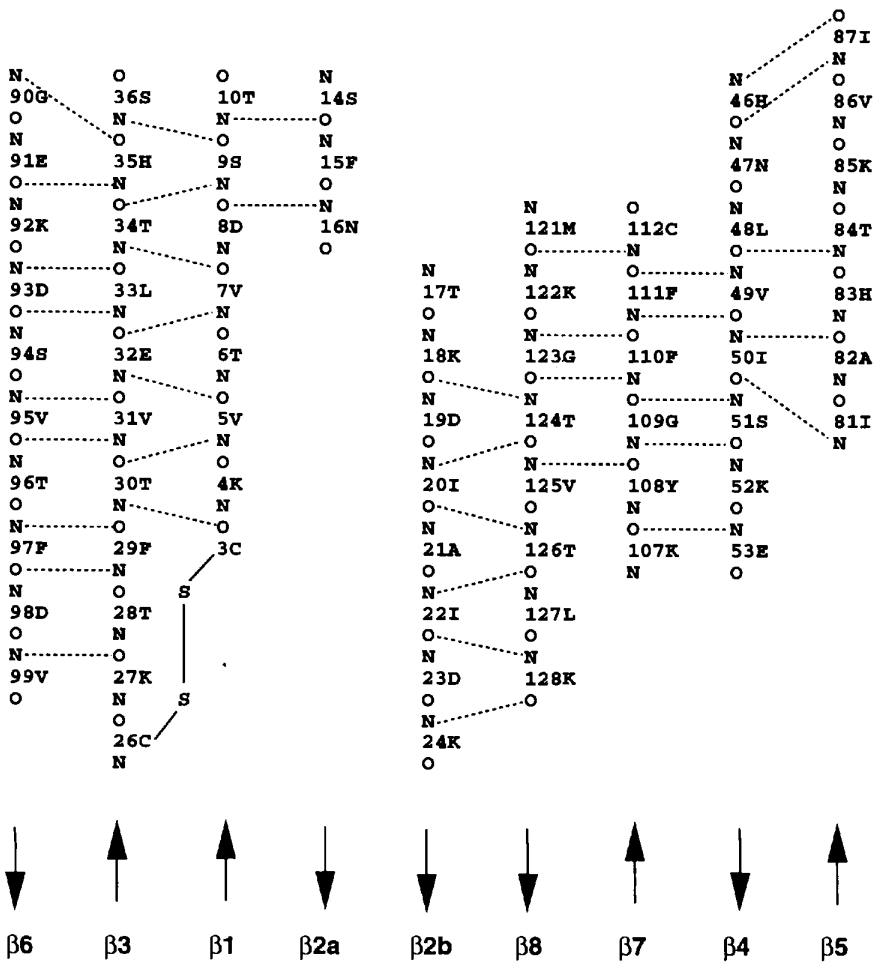

Fig. 11. Main-chain secondary structure of *P. putida* azurin. Hydrogen bonds are indicated by dashed lines connecting donors and acceptors. β-strand polarities are indicated with arrows. The unique disulfide bridge Cys3–Cys26 is shown by solid lines.

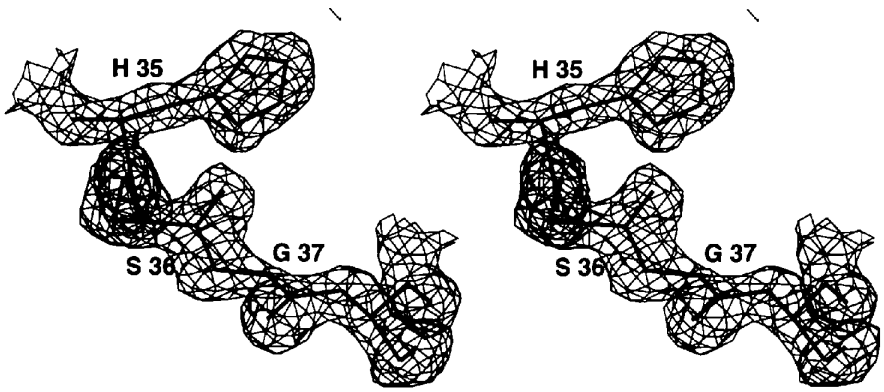

Fig. 12. Stereoview of the $2F_o - F_c$ electron-density map showing the interaction between His35 $N^{\delta 1}$ and Ser36 O in zinc azurin at 1.6 Å resolution. The map is contoured at 1.0σ.

other conserved side-chain-to-side-chain intramolecular hydrogen bonds, those between residues 23 and 25, 30 and 96, 47 and 113, and 10 and 14. The first two are hydrogen bonds between invariant residues and the remaining two are between similar residues in these azurins. Five other hydrogen bonds which are located on the surface of PP azurin, Asp8 $O^{\delta 2}\cdots$Ser36 O^{γ}, Asp8 $O^{\delta 1}\cdots$Thr34 $O^{\gamma 1}$, Asp19 $O^{\delta 1}\cdots$Thr124 $O^{\gamma 1}$, Asp19 $O^{\delta 1}\cdots$Thr126 $O^{\gamma 1}$ and Gln57 $O^{\varepsilon 1}\cdots$Thr61 $O^{\gamma 1}$, are not present in any of the other three azurins. On the other hand, two hydrogen bonds, between positions 32 and 94, and between positions 106 and 108 are not formed in PP azurin but exist in azurin from both AD and PA. The intermolecular hydrogen-bond interactions in native azurin are listed in Table 4. Three long salt bridges are formed between Lys18*A* N^{ζ}—Asp93*A*# $O^{\delta 1}$, Glu53*A* $O^{\varepsilon 1}$ and $O^{\varepsilon 2}\cdots$Lys92*A*# N^{ζ}, and Lys70*A* N^{ζ}—Asp93*B*# $O^{\delta 1}$ and $O^{\delta 2}$. Table 5 lists the intermolecular hydrogen-bond interactions in zinc azurin. There are two well defined salt bridges, Lys70*A* N^{ζ}—Asp93*B*# $O^{\delta 1}$ (2.58 Å) and Glu2*A* $O^{\varepsilon 1}$—Lys74*B*# N^{ζ} (2.69 Å). The latter is located close to the N terminus. The salt bridge between Glu2*A* $O^{\varepsilon 2}$ and Arg79*B*# $N^{\eta 1}$ (3.24 Å) and between Glu2*B* $O^{\varepsilon 2}$ and Lys70*B*# N^{ζ} are weaker and are close to the N termini. A total of 163 and 222 water molecules have been located in the native and zinc-azurin structures, respectively. The average *B* values for water molecules in native and zinc azurins are 40.4 and 32 Å^2, respectively. Occupancies were not refined. Like azurin from AD, there are no truly internal water molecules in PP azurin. Many well ordered water molecules with low *B* factor (<30 Å^2 for native azurin, <25 Å^2 for zinc azurin) are located in deep pockets on the protein surface, and are mostly in equivalent positions in the two molecules of each structure, forming two or three strong hydrogen bonds, mostly with main-chain carbonyl O and amide N atoms.

In addition to the water molecules in the dimer interface described above, there is another water molecule, bound to the solvent exposed $N^{\varepsilon 2}$ of His83 in both native PP azurin molecules in the asymmetric unit which is quite interesting. In zinc azurin both water molecules of the dimer are replaced by zinc ions (see below). In the azurin structure from AD, a sulfate ion is bound to His83, while a check of the solvent structure of azurin from PA reveals a water molecule bound to His83 in three of the four monomers. It is notable that above the His83 side chain there are more than 15 water molecules hydrogen bonded to each other which lie in a wide depression in each molecule of zinc azurin. In native azurin, there are six to eight water molecules also located above this side chain and a similar situation exists in AD azurin (Baker, 1988).

3.6. *Zinc binding*

The difference map for the zinc azurin, computed before any solvent was introduced, showed four peaks above 9σ while the smoothly diminishing noise peaks started below 7σ. When refined as water, their *B* values were all near 2.0 Å^2. All four peaks have been modeled as zinc during the refinement.

Zinc site 1 is located on a non-crystallographic twofold axis. This axis relates a pair of azurin monomers in a tail-to-tail manner. The coordination is nearly octahedral, with ligands comprised of $O^{\delta 1}$ from Asp23*A* and O^{γ} from Ser25*A*, as well as of the NCS-related pair of side chains, and two water molecules (Table 6, Fig. 13). Zinc site 2 is bound to $N^{\varepsilon 2}$ of a single histidine at position 83*B* and is further coordinated by five water molecules. Zinc site 3 is 5-coordinate, liganded by $N^{\varepsilon 2}$ of His83*B* and both carboxylates of Asp69*A*# of a symmetry-related molecule

Table 4. *Intermolecular interactions in native azurin*

Atom *X*	Atom *Y*	Distance (Å)
Lys18*A* N^{ζ}	Asp93*A* $O^{\delta 1}$ (vi)	3.16
Lys18*A* N^{ζ}	Ser94*A* O (vi)	3.03
Lys27*A* N^{ζ}	Ser38*B* O^{γ} (ii)	3.21
Glu53*A* $O^{\varepsilon 1}$	Lys92*A* N^{ζ} (v)	3.16
Glu53*A* $O^{\varepsilon 2}$	Lys92*A* N^{ζ} (v)	3.22
Ala66*A* O	Lys85*B* N^{ζ} (v)	2.81
Lys70*A* N^{ζ}	Asp93*B* $O^{\delta 1}$ (iv)	3.22
Lys70*A* N^{ζ}	Asp93*B* $O^{\delta 2}$ (iv)	2.95
Lys75*A* $O^{\delta 2}$	Ser94*B* O^{γ} (iii)	3.29
Asp75*A* $O^{\delta 2}$	Thr96*B* $O^{\gamma 1}$ (iii)	2.83
Asp75*A* $O^{\delta 1}$	Thr96*B* N (iii)	2.79
Gly76*A* O	Lys18*B* N^{ζ} (i)	2.92
Gly90*A* O	Lys107*A* N^{ζ} (iv)	3.28

Symmetry operators: (i) $(x+1, y, z)$; (ii) $(-x, y+\frac{1}{2}, -z)$; (iii) $(-x+1, y+\frac{1}{2}, -z)$; (iv) $(-x+1, y+\frac{1}{2}, -z+1)$; (v) $(-x, y+\frac{1}{2}, -z)$; (vi) $(-x+1, y+\frac{1}{2}, -z)$.

Table 5. *Intermolecular interactions in zinc azurin*

Atom *X*	Atom *Y*	Distance (Å)
Glu2*A* $O^{\varepsilon 1}$	Lys74*B* N^{ζ} (ii)	2.69
Glu2*A* $O^{\varepsilon 2}$	Arg79*B* $N^{\eta 1}$ (ii)	3.24
Lys18*A* N^{ζ}	Ser94*A* O^{γ} (vii)	3.15
Ser25*A* O^{γ}	Lys128*B* $O^{\tau 1}$ (iii)	2.76
Ser38*A* O^{γ}	Ser100*A* O^{γ} (iv)	3.07
Asn42*A* $N^{\delta 2}$	Met120*B* S^{δ}	2.91
Lys52*A* N^{ζ}	Gln12*B* $O^{\varepsilon 1}$ (i)	3.17
Ser65*A* O	Lys85*B* N^{ζ} (vi)	2.78
Lys70*A* N^{ζ}	Asp93*B* $O^{\delta 1}$ (vi)	2.58
Lys70*A* N^{ζ}	Asp93*B* $O^{\delta 2}$ (vi)	3.21
Lys70*A* N^{ζ}	Ser94*B* O (vi)	3.20
Lys74*A* N^{ζ}	Asn16*B* O (ii)	3.17
Asp75*A* $O^{\delta 2}$	Ser94*B* O^{γ} (v)	3.25
Asp75*A* $O^{\delta 2}$	Thr96*B* $O^{\gamma 1}$ (v)	2.81
Asp75*A* $O^{\delta 1}$	Thr96*B* N (v)	3.01
Lys128*A* $O^{\tau 1}$	Ser25*B* O^{γ} (iii)	2.75
Glu2*B* $O^{\varepsilon 1}$	Lys70*B* N^{ζ} (ii)	2.93
Glu2*B* $O^{\varepsilon 2}$	Lys70*B* N^{ζ} (ii)	3.18
Gln57*B* $N^{\varepsilon 2}$	Asp69*B* $O^{\delta 1}$ (vi)	3.20

Symmetry operators: (i) $(x, y+1, z)$; (ii) $(x+1, y, z)$; (iii) $(x+1, y+1, z)$; (iv) $(-x+1, y+\frac{1}{2}, -z)$; (v) $(-x+1, y+\frac{1}{2}, -z+1)$; (vi) $(-x+2, y-\frac{1}{2}, -z+1)$; (vii) $(-x+2, y+2\frac{1}{2}, -z+2)$.

Table 6. *Coordination geometry of the zinc sites of azurin*

= crystallographic symmetric operation.

Zinc site 1					
Zn—ligand bond lengths (Å)					
$O^{\delta 1}$(D23*A*)—Zn	2.16	O^{γ}(S25*A*)—Zn	2.21	$O^{\delta 1}$(D23*B*#)—Zn	2.14
Wat(653)—Zn	2.31	O^{γ}(S25*B*#)— Zn	2.10	Wat(571)—Zn	2.14
Ligand—Zn—ligand bond angles (°)					
$O^{\delta 1}$(D23*A*)—Zn—O^{γ}(S25*A*)	87.87	O^{γ}(S25*A*)—Zn—Wat(571)	172.22		
Wat(571)—Zn—$O^{\delta 1}$(D23*B*#)	98.44	$O^{\delta 1}$(D23*B*#)—Zn—Wat(653)	92.02		
Wat(653)—Zn—O^{γ}(S25*B*#)	169.66	O^{γ}(S25*B*#)—Zn—$O^{\delta 1}$(D23*A*)	85.00		
O^{γ}(S25*B*#)—Zn—Wat(571)	86.47	$O^{\delta 1}$(D23*A*)—Zn—$O^{\delta 1}$(D23*B*#)	169.10		
O^{γ}(S25*A*)—Zn—Wat(653)	88.90	O^{γ}(S25*B*#)—Zn—$O^{\delta 1}$(D23*B*#)	91.40		
$O^{\delta 1}$(D23*B*#)—Zn—O^{γ}(S25*A*)	82.74	O^{γ}(S25*B*#)—Zn—O^{γ}(S25*A*)	101.21		
$O^{\delta 1}$(D23*A*)—Zn—Wat(653)	93.31	$O^{\delta 1}$(D23*A*)—Zn—Wat(571)	91.62		
Wat(653)—Zn—Wat(571)	83.38				
Zinc site 2					
Zn—ligand bond lengths (Å)					
$N^{\epsilon 2}$(H83*A*)—Zn	2.04	Wat(646)—Zn	2.32	Wat(632)—Zn	2.16
Wat(618)—Zn	1.95	Wat(713)—Zn	1.93	Wat(606)—Zn	2.77
Zinc site 3					
Zn—ligand bond lengths (Å)					
$N^{\epsilon 2}$(H83*B*)—Zn	2.01	$O^{\delta 2}$(D69*A*#)—Zn	2.29	$O^{\delta 1}$(D69*A*#)—Zn	2.43
Wat(537)—Zn	2.12	Wat(513#)—Zn	2.25		
Zinc site 4					
Zn—ligand bond lengths (Å)					
$O^{\delta 2}$(D62*B*)—Zn	2.07	$O^{\epsilon 1}$(E2*A*#)—Zn	3.01	Wat(525)—Zn	2.34
$O^{\delta 1}$(D62*B*)—Zn	2.82	$O^{\epsilon 2}$(E2*A*#)—Zn	2.38	Wat(622#)—Zn	2.30

and by two water molecules. Zinc site 4 is coordinated by both carboxylates of Glu2*A*# and of Asp62*B* plus two water molecules.

The assignment of the four zinc sites in zinc azurin is based on the large magnitude of the difference density peaks and on their high coordination number. Three of the sites have six ligands while the remaining one has five. The average coordination distance for the first three zinc sites is 2.2 Å. For the fourth site the average coordination distance is 2.5 Å. It is reasonable to assign these four sites described here to zinc since it was the only additional cation present during crystallization compared with the native protein. Site 2 might be suspect since it has only one protein ligand, but it has a high coordination number at a short distance and is closely related to site 3 by non-crystallographic symmetry. Site 4 is 6-coordinate, but has somewhat longer coordination distances than the others. It is unlikely to be the site for another type of metal ion since no metals others than zinc and sodium were present during crystallization, and the magnitude of the electron density for the site appears to be too great to be sodium.

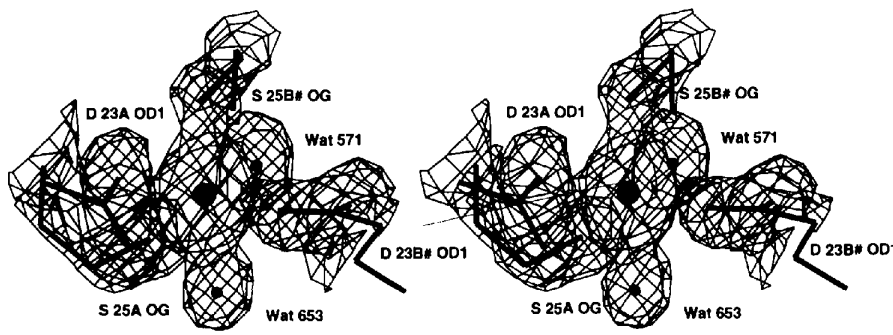

Fig. 13. Stereoview of the $2F_o - F_c$ electron-density map centered on Zn1 of zinc azurin at 1.6 Å resolution. The map is contoured at 1.0σ. The Zn ion, shown as a large filled circle, is located on the non-crystallographic twofold axis. It has six ligands which form an approximate octahedron, two from $O^{\delta 1}$ of Asp23*A* and Asp23*B*#, two from O^{γ} of Ser25*A* and Ser25*B*#, and two from water (shown as small filled circles). The symbol # indicates a crystallographically related side chain.

In both crystal lattices the azurin 'dimers' of the asymmetric unit are arranged in layers perpendicular to the b axis. The monomers of the non-crystallographic 'dimer' make a V-angle of about 50° between the principal axes of the β-barrels with the planes of the V's lying parallel to the layers. The unit cell of azurin is composed of two non-crystallographic 'dimers' related by a crystallographic twofold screw axis parallel to b and located at $x = a/2$ and $z = c/2$. The crystal packing of the native and zinc azurins within their respective unit cells is very similar, with r.m.s. deviations of 0.77 Å for 512 equivalent C atoms when the complete unit cells are superimposed.

The lengths of the b and c axes are very similar in the crystals of native and zinc azurins, differing by approximately 0.4 Å (Table 1). Because of this, the repeating pattern of unit cells in the y and z directions is quite similar for the two types of crystals, resulting in homologous interactions between neighboring molecules. However, the a axes differ by about 2.5 Å and the β angle by about 4.5°. The main cause for this difference is the change in crystal packing along the (−101) direction caused by the presence of zinc site 1 in the lattice of zinc azurin. This site is located on the alternate non-crystallographic twofold axes between dimers within the same layer of molecules and translated by one unit along the $-a$ and $+c$ directions. This leads to the largest difference between the native and zinc azurin unit cells, a shrinking by nearly 4 Å along the (−101) diagonal of the unit cell (Fig. 14) The binding of the zinc ion at site 1 pulls the two dimers together, reducing the distance between Asp23 CA and Asp23# CA by 3.7 Å so that the carboxylate side chains of zinc azurin are separated by 4.3 rather than 8.1 Å as in the native. At this reduced distance, the strong interactions between the two dimers shown in Fig. 10 can form.

The other three zinc binding sites have little effect on the crystal packing of the two forms of azurin. Zinc site 2 is coordinated only to molecule *A* plus five water molecules. Zinc site 3 is coordinated to a side chain of molecule *B* and to two atoms from a twofold screw-related molecule *A* which pack similarly in the native and zinc unit cells. Although zinc sites 2 and 3 are related by a non-crystallographic twofold axis, their lattice contacts result from crystallographic twofold screw symmetry operations and are quite different. The zinc ion at site 4 is located between unit cells separated by a translation along c which differs little between native and zinc azurins, the distance between the Cα atoms of the ligands Glu2*A*# and Asp62*B* being 10.46 and 10.16 Å, respectively.

4. Discussion

The native and zinc *P. putida* azurins are very similar in structure. The latter structure, at 1.6 Å resolution, has been determined at the highest resolution so far observed for an azurin, and reveals considerable structural detail. The structure of the *P. putida* azurin molecule is also quite similar to the other known azurins from *A. denitrificans*, *P. aeruginosa* and *A. xylosoxidans*. The fivefold coordination of the copper site is a well conserved feature of the azurin family.

Azurin from *P. aeruginosa* undergoes a pH-dependent protonation/deprotonation of His35 $N^{\delta 1}$ which is correlated with a Pro36–Gly37 peptide flip. At low pH (as observed in crystals at pH 5.5; Nar *et al.*, 1991*a*) Pro36 O receives a hydrogen bond from the protonated His35 $N^{\delta 1}$ while at high pH (observed in crystals at pH 9.0) Gly37 N donates a hydrogen bond to the deprotonated His35 $N^{\delta 1}$. AD azurin does not display a pH-dependent isomerization and its structure (determined at pH 5.0; Baker, 1988), as well as the structure of AX azurin (determined at pH 6.0; Dodd *et al.*, 1995) indicate that His35 $N^{\delta 1}$ is unprotonated. It was postulated (Adman, 1985; Nar *et al.*, 1991*a*) that in AD azurin, a hydrogen bond formed between Val36 N and Ser9 O leads to a constriction of the pocket containing the His35 side chain which prevents protonation of the $N^{\delta 1}$ from occurring, while in PA, the presence of proline at position 36 prevents formation of that hydrogen bond. In the PP azurin structures (both native and zinc forms) His35 is protonated, even though the Ser36 N to Ser9 O hydrogen bond is maintained and despite the higher pH of 7.0–7.5 under which the PP azurin crystals were grown. The difference between the protonation states of His35 in AD and PP azurins must arise from a more subtle combination of structural differences between the two proteins. It will be of interest to determine whether PP azurin undergoes any pH-dependent isomerization linked to the His35 position.

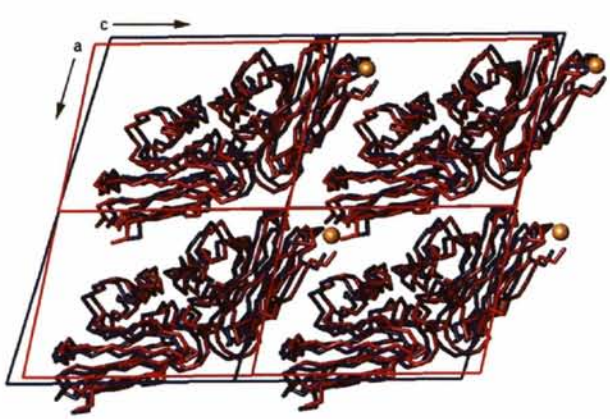

Fig. 14. Crystal packing arrangement of a single layer of 'head-to-head' dimers of azurin (blue) and zinc azurin (red) molecules lying perpendicular to the crystallographic b axes of the four unit cells (also shown in blue and red, respectively). Four zinc ions, one associated with each zinc azurin dimer and located on the non-crystallographic symmetry dyads, are shown as large yellow spheres. One of these is shown connecting two dimers in a 'tail-to-tail' arrangement in adjacent unit cells in the (−101) direction. The interactions between zinc azurin dimers stabilized by the zinc ion pull the molecules closer together in the diagonal direction than in the native azurin and explains the change in unit-cell parameters.

The interactions within the 'head-to-head' dimer of the two azurin molecules in the asymmetric unit appear to be stable and specific, since these interactions are observed in two different crystal lattices, with low (0.4 Å) r.m.s. deviation of Cα atoms between the dimers. An analogous dimer, although different in structure, is stable and specific in the PA structure as well, where two nearly identical dimers occur in the asymmetric unit. In the azurin crystal structures so far determined, 'head-to-head' dimerization has been observed. Though in all cases the interaction is through the hydrophobic residues surrounding the copper ligand His117, the mode of association can be divided into three categories with radically different relative orientations. These differences in orientations range from 45 to 150° and result in permutations of the interactions of hydrophobic loops between molecules, but all dimers maintain a Cu—Cu distance of about 15 Å. Thus, there appears to be a multiplicity of stable interactions between azurin molecules, any or all of which may result in complexes capable of productive electron self exchange.

The 'tail-to-tail' arrangement of the PP zinc azurin is strongly influenced by the binding of the zinc ion. The packing of monomers within the unit cells of native and zinc azurins is nearly the same (0.77 Å r.m.s. deviation) and the packing of unit cells in the crystallographic *b* direction is also quite similar. The presence of the zinc ion in zinc azurin leads to a very strong association between molecules involving the interactions of three side chains from each molecule, two water molecules and the zinc ion. The principle effect of this association is to shorten the lattice translation by about 4 Å in the (−101) diagonal direction concomitant with at reduction of the β angle by over 4°. The tighter association between the azurin molecules in zinc azurin reduces the mobility of certain chain segments and appears to have the added benefit of increasing the crystalline order, leading to the capability of recording data at higher resolution than with the native structure.

We thank Dr R. C. E. Durley, Dr L. M. Cunane and Dr J. D. Barton for helpful discussions. This work was supported by USPHS grants No. GM20530 (FSM), GM32696 (MJB) and HL16251 (WSM), and by a Department of Veterans Affairs Merit Review Grant and an Academic Senate and Research Evaluation and Allocation Committee Grant, University of California San Francisco (WSM). Access to a multi-processor computer server was provided through NIH grant No. RR10412. Atomic coordinates and structure factors have been deposited with the Protein Data Bank.†

† Atomic coordinates and structure factors have been deposited with the Protein Data Bank, Brookhaven National Laboratory (Reference: 1NWO, R1NWOSF and 1NWP, R1NWPSF). Free copies may be obtained through The Managing Editor, International Union of Crystallography, 5 Abbey Square, Chester CH1 2HU, England (Reference: AM0057)

References

Adman, E. T. (1985). *Metalloproteins*, edited by P. M. Harrison, Vol. 1, pp. 1–42. Weinheim, Germany: Verlag Chemie.

Adman, E. T. (1991). *Adv. Protein Chem.* **42**, 145–197.

Adman, E. T. & Jensen, L. H. (1981). *Isr. J. Chem.* **21**, 8–12.

Baker, E. N. (1988). *J. Mol. Biol.* **203**, 1071–1095.

Baker, E. N. & Hubbard, R. E. (1984). *Prog. Biophys. Mol. Biol.* **44**, 97–179.

Barber, M. J., Trimboli, A. J. & McIntire, W. S. (1993). *Arch. Biochem. Biophys.* **303**, 22–26.

Barton, G. J. (1993). *Protein Eng.* **6**, 37–40.

Bernstein, F. C., Koetzle, T. F., Williams, G. J. B., Meyer, E. F., Brice, M. D., Rodgers, J. R., Kennard, O., Shimanouchi, T. & Tasumi, M. (1977). *J. Mol. Biol.* **112**, 535–542.

Blackwell, K. A., Anderson, B. F. & Baker, E. N. (1994). *Acta Cryst.* D**50**, 263–270.

Brünger, A. T. (1992*a*). *X-PLOR Manual, Version* 3.1, Yale University Press, New Haven, CT, USA.

Brünger, A. T. (1992*b*). *Nature (London)*, **355**, 472–475.

Brünger, A. T. (1993). *Acta Cryst.* D**49**, 24–36.

Causer, M. J., Hopper, D. J., McIntire, W. S. & Singer, T. P. (1984). *Biochem. Soc. Trans.* **12**, 1131–1132.

Chen, L., Durley, R. C. E., Mathews, F. S. & Davidson, V. L. (1994). *Science*, **264**, 86–90.

Chen, L., Mathews, F. S., Davidson, V. L., Tegoni, M., Rivetti, C. & Rossi, G. L. (1993). *Protein Sci.* **2**, 147–154.

Connolly, M. J. (1983). *J. Appl. Cryst.* **24**, 548–558.

Cunane, L. M., Chen, Z., Durley, R. C. E. & Mathews, F. S. (1996). *Acta Cryst.* D**52**, 676–686.

Dodd, F. E., Hasnain, S. S., Abraham, Z. H. L., Eady, R. R. & Smith, B. E. (1995). *Acta Cryst.* D**51**, 1052–1064.

Edwards, S. L., Davidson, V. L., Hyun, Y.-L. & Wingfield, P. T. (1995). *J. Biol. Chem.* **270**, 4293–4298.

Engh, R. A. & Huber, R. (1991). *Acta Cryst.* A**47**, 392–400.

Farver, O., Skov, L. K., Pascher, T., Karlsson, B. G., Nordling, M., Lundberg, L. G., Vänngard, T. & Pecht, I. (1993). *Biochemistry*, **32**, 7317–7322.

Fitzgerald, P. M. D. (1988). *J. Appl. Cryst.* **21**, 273–278.

Hamlin, R. (1985). *Methods Enzymol.* **114**, 416–452.

Hammann, C., Messerschmidt, A, Huber, R., Nar, H., Gilardi, G. & Canters, G. W. (1996). *J. Mol. Biol.* **255**, 362–366.

Hendrickson, W. A. & Konnert, J. H. (1980). *Biomolecular Structure, Function, Conformation and Evolution*, Vol. 1, edited by R. Srinivasan, pp. 43–57. Oxford: Pergamon Press.

Jones, T. A. (1985). *Methods Enzymol.* **115**, 157–171.

Kabsch, W. & Sander, C. (1993). *Biopolymers*, **22**, 2577–2637.

van de Kamp, M., Silvestrini, M. C., Brunori, M., Van Beeumen, J., Hali, F. C. & Canters, G. W. (1990). *Eur. J. Biochem.* **194**, 109–118.

Korszun, Z. R. (1987). *J. Mol. Biol.* **196**, 413–419.

Laskowski, R. A., MacArthur, M. W., Moss, D. S. & Thornton, J. M. (1993). *J. Appl. Cryst.* **26**, 283–291.

Matthews, B. W (1968). *J. Mol. Biol.* **33**, 491–497.

Murphy, L. M., Strange, R. W., Karlsson, B. G., Lundberg, L. G., Pascher, T., Reinhammar, B. & Hasnain, S. S. (1993). *Biochemistry*, **32**, 1965–1975.

Nar, H., Huber, R., Messerschmidt, A., Filippou, A. C., Barth, M., Jaquinod, M., van De Kamp, M. & Canters, G. W. (1992). *Eur. J. Biochem.* **205**, 1123–1129.

Nar, H., Messerschmidt, A., Huber, R., van de Kamp, M. & Canters, G. W. (1991*a*). *J. Mol. Biol.* **221**, 765–772.

Nar, H., Messerschmidt, A., Huber, R., van de Kamp, M. & Canters, G. W. (1991*b*) *J. Mol. Biol.* **218**, 427–447.

Nar, H., Messerschmidt, A., Huber, R., van de Kamp, M. & Canters, G. W. (1992). *FEBS Lett.* **306**, 119–124.

Norris, G. E., Anderson, B. F. & Baker, E. N. (1983). *J. Mol. Biol.* **165**, 501–521.

Romero, A., Hoitink, C. W. G., Nar, H., Huber, R., Messerschmidt, A. & Canters, G. W. (1993). *J. Mol. Biol.* **229**, 1007–1021.

Strange, R. W., Murphy, L., Karlsson, B. G., Lindley, P. F., Lundberg, L. G., Reinhammar, B. & Hasnain, S. S. (1994). *Acta Cryst.* D**50**, 37–39.

Tsai, L., Sjölin, L., Langer, V., Bonander, N., Karlsson, B. G., Vänngård, T., Hammann, C. & Nar, H. (1995). *Acta Cryst.* D**51**, 711–717.

Tsai, L., Sjölin, L., Langer, V., Pascher, T. & Nar, H. (1995). *Acta Cryst.* D**51**, 168–176.

Wilson, A. J. C. (1949). *Acta Cryst.* **2**, 318.

Wlodawer, A., Hodgson, K. O. & Shooter, E. M (1975). *Proc. Natl Acad. Sci. USA*, **72**, 777–779.

Zhu, D. W., Dahms, T., Willis, K., Szabo, A. G. & Lee, X. (1994). *Arch. Biochem. Biophys.* **308**, 469–470.